Applied Catalysis B: Environmental 325 (2023) 122363

Contents lists available at ScienceDirect

Applied Catalysis B: Environmental

journal homepage: www.elsevier.com/locate/apcatb

Quantifying nitroaromatics via terminating their photoreduction catalyzed by Eosin Y

Jing-Hang Wu [1], Tian-Hao Yang [1], Fei Chen, Feng Zhang, Jie-Jie Chen, Han-Qing Yu [*]

CAS Key Laboratory of Urban Pollutant Conversion, Department of Environmental Science and Engineering, University of Science and Technology of China, Hefei 230026, China

ARTICLE INFO

Keywords:
Nitroaromatic compounds
Quantitation
Eosin Y
Catalytic reduction
Photobleaching kinetics
Colorimetric method

ABSTRACT

The environmental and safety concerns caused by nitroaromatic compounds (NACs) require a sensitive, reliable, and easy-to-use method for their detection. In this work, we observed that an ultrafast photobleaching occurred when the photoreduction of NACs catalyzed by eosin Y (EY) was terminated. Based on such a semi-cycle photocatalysis, a colorimetric method was developed to quantify NACs with a linear relationship between the pseudo-first-order kinetic constant (k_{app}) of EY photobleaching and NACs concentration. This method exhibited a high sensitivity, low detection limit (6.57 ppb), and good anti-interference ability in the presence of various ions or organics in water matrices, enabling satisfactory quantification results for practical water samples. Moreover, the EY-based photocatalysis mechanisms inspires that the ultra-fast EY decoloration in the NAC solution was attributed to the fragment of the photoexcited EY molecule. This work provides a feasible photocatalysis-based NAC detection approach by applying a "off-the-shelf" probe.

1. Introduction

Nitrobenzene (NB) is an important industrial raw material [1], and derives a variety of nitroaromatic compounds (NACs) that are commonly used as explosives [2], pharmaceutical intermediates [3], and dye precursors [4]. Moreover, NACs and their transformation products in the environment may be carcinogenic and teratogenic [5]. The wide use of these NACs raises environmental, health, and safety concerns, and thus, sensitive NAC detection is required to reveal their potential risks [6,7]. Conventional methods mainly include chromatographic and colorimetric assays. Such methods are somewhat effective but possibly limited by high cost or poor accuracy [8]. Thus, a reliable and low-cost method for the highly sensitive detection of NAC in complex water matrices is highly desired.

Some emerging electrode materials such as metal-organic frameworks have been proposed to electrochemically respond to NACs, enabling quantitative analysis of NAC concentrations [9]. In addition, various spectral methods have been developed by designing different colorimetric, fluorescent, or luminescent probes to avoid using expensive electrochemical systems [10]. These methods show a lower detection limit (LoD) than conventional electrochemical methods [11–13]. However, most of these electrode materials and probes were explicitly fabricated and relatively laborious [14,15], further limiting their widespread use and standardization [16]. New approaches to select probes in commercially available materials will facilitate their practical application.

To date, various catalytic approaches have been developed to reduce the $-NO_2$ groups in NACs [17–19] as NAC reduction is recognized as a key intermediate stage for synthesizing various high-value-added compounds [20]. Inspiringly, spectral monitoring of catalyst may enable a selective detection for the corresponding substrate [21]. Developing such a catalyst for NAC reduction as a probe may provide (i) a high-selectivity half-reaction, (ii) a clear description of the corresponding photocatalytic mechanism, and (iii) an excellent spectral response. Thus, the change in such a photocatalyst may accumulate by terminating the electron supply to stop the photocatalytic cycle and is monitored to indicate the presence of NAC substances. Generally, soluble photocatalysts also exhibit good spectral response, e.g., Eosin Y (EY), a widely studied and commercially available organo-photocatalyst for synthetic conversions [22]. Moreover, EY enables mild and selective photocatalytic NAC reduction in aerobic aqueous solution in the presence of dissolved oxygen [23]. Reportedly, NB can efficiently quench the

* Corresponding author.
E-mail address: hqyu@ustc.edu.cn (H.-Q. Yu).
[1] The authors contributed equally to this work.

https://doi.org/10.1016/j.apcatb.2023.122363
Received 8 August 2022; Received in revised form 4 October 2022; Accepted 2 January 2023
Available online 3 January 2023

triplet excited state of EY (EY*), and it is used as a specific oxidant in EY-catalyzed photoreduction [24,25]. During EY photocatalysis, defects due to its poor stability have been widely studied [26]. In contrast, the selective destruction of chromophores will indicate the presence of NACs, while quantitative analysis of NAC concentration may be further provided by kinetic aspects.

In this work, rapid photoinduced fragmentation of the eosin chromophore in the presence of NACs was found, leading to complete decolorization and a significant decrease in absorption. Then, the possible mechanism of this newly discovered dye fragmentation in the semi-cycle photocatalysis was investigated, demonstrating the structural dependence of NAC-catalyzed dye photobleaching. After that, a new method was established to quantify the NAC concentrations by using UV–Vis spectroscopy for the kinetic analysis of such a selective

Table 1
Dyes used as the probes for detecting NACs in this work.

Name	Structure	Chemical formula	Abbreviation
eosin Y	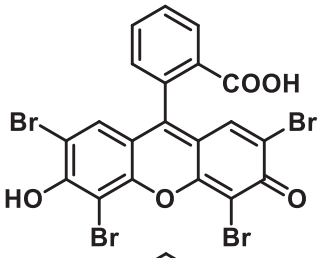	$C_{20}H_8Br_4O_5$	EY
fluorescein	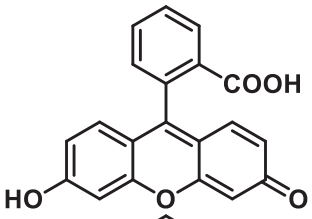	$C_{20}H_{12}O_5$	FL
4,5-dichloro-fluorescein	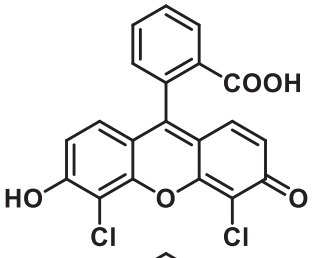	$C_{20}H_{10}Cl_2O_5$	DCF
4,5-dibromo-fluorescein	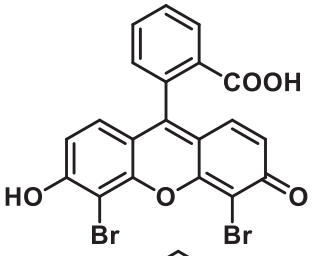	$C_{20}H_{10}Br_2O_5$	DBF
eosin B	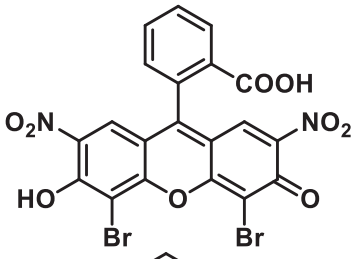	$C_{20}H_8Br_2N_2O_9$	EB
erythrosin B	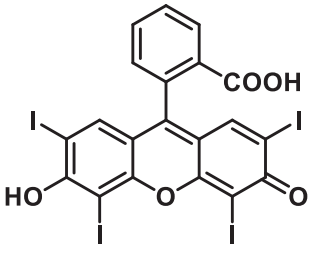	$C_{20}H_8I_4O_5$	ErB

(continued on next page)

Table 1 (*continued*)

Name	Structure	Chemical formula	Abbreviation
phloxine B	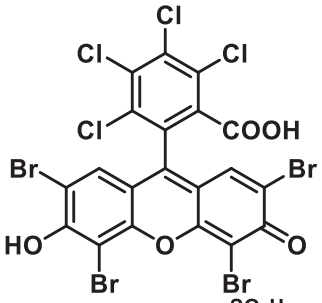	$C_{20}H_4Br_4Cl_4O_5$	PB
light green SF	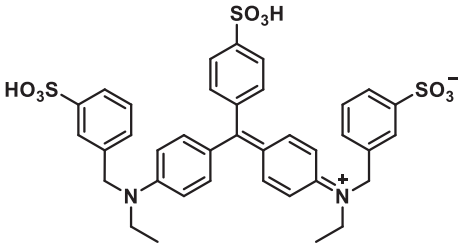	$C_{37}H_{36}N_2O_9S_3$	LG
acriflavine	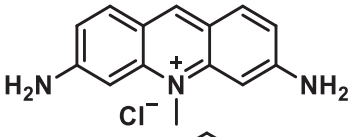	$C_{14}H_{14}N_3Cl$	AF
rhodamine B	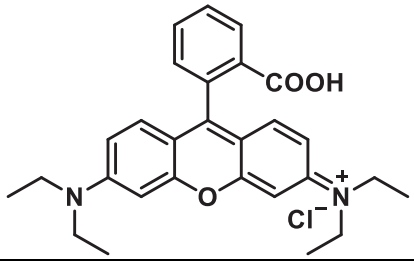	$C_{28}H_{31}ClN_2O_3$	RhB

NAC-induced EY decolorization. Finally, the sensitivity, selectivity, robustness, and feasibility of the proposed NAC detection method in practical water matrices were comprehensively evaluated. The approach of developing probes from photocatalytic systems will facilitate the practical application and standardization of spectral detection of targeting environmental pollutants.

2. Materials and methods

2.1. Chemicals and reagents

Unless otherwise stated, all reagents used in this work were purchased from Aladdin Reagent Co., China. The dyes and NACs used in this work are listed in Tables 1 and 2, respectively. Moreover, the detailed informations on these compounds can be found in the Supplementary Materials.

2.2. Photocatalytic tests

In a typical photobleaching test, the EY solution containing nitrobenzene was irradiated with a 6 W LED light source ($\lambda = 525$ nm, green). After a certain reaction time, the UV–Vis spectra were recorded with a UV-2550 spectrophotometer (Shimadzu Co., Japan). For kinetic studies, the absorbance at 517 nm (the maximum absorbance of EY) was used to indicate the EY concentrations [27,28]. The photobleaching experiments of other dyes were conducted under irradiation with a 300 W Xenon lamp (PLS-SXE 300D/300DUV, Beijing Perfectlight) with a 400 nm cutoff filter. Moreover, the transient photocurrent responses were obtained by a modified photoelectrochemical measurement method for heterogeneous photocatalysts (Supplementary Materials, Text S1) [29]. The irradiation intensities were measured with a digital optical power meter (PM100D, Thorlabs Inc., USA).

2.3. Analysis

The photobleaching products were detected by liquid chromatography coupled with a mass spectrometer (LC–MS, AB Triple TOF 5600 +, AB Sciex Co., USA) and analyzed using an Xbridge BEH C18 column (2.5 μm, 2.1 mm × 100 mm, Waters In., USA). The eluent consisted of acetonitrile (eluent A) and 0.1% formic acid water (eluent B) at a flow rate of 0.3 mL·min^{-1}. The gradient program for the volume ratios was as follows: 0–3 min, 95% A; 3–8 min, 95–50% A; 8–10 min, 50%; 10–11 min, 50–5%; 11–17 min, 5%; 17–18 min, 5–95%; 18–20 min, 95%. A scan range of m/z 50–600 was selected in both positive and negative modes. The experimental parameters for three-dimensional fluorescence spectra and electron paramagnetic resonance spectra are detailed in Supplementary Materials.

Table 2
NACs used in this work.

Name	Structure	Chemical formula	Abbreviation
nitrobenzene	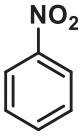	$C_6H_5NO_2$	NB
2-nitrotoluene	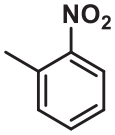	$C_7H_7NO_2$	NT
4-nitrophenol	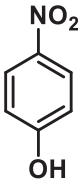	$C_6H_5NO_3$	NP
4-nitroaniline	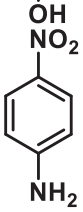	$C_6H_6N_2O_2$	NA
1-chloro-4-nitrobenzene	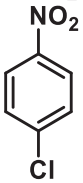	$C_6H_4ClNO_2$	CNB
1-bromo-2-nitrobenzene	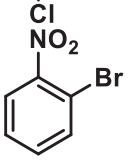	$C_6H_4BrNO_2$	BNB
4-nitrophenylacetonitrile	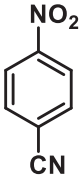	$C_7H_4N_2O_2$	NPA
2,4-dinitrotoluene	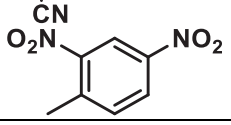	$C_7H_6N_2O_4$	DNT

2.4. Computational methods

All calculations were performed with Gaussian 16. The first twenty excited states were determined using perturbative TD-DFT to generate UV–Vis spectra. In addition, the energies of the highest occupied molecular orbital (HOMO) and the lowest unoccupied molecular orbital (LUMO) were determined at the B3LYP/6–31 + +g(d,p) level. Details of the calculations are provided in Supplementary Materials (**Text S4**).

2.5. Water samples

Actual water samples from natural and artificial water sources were collected and tested in May 11 2022. Samples from Chaohu Lake (31°40'44.4" N, 117°26'29.0" E and 31°32'30.9" N, 117°28'26.4" E), Hefei, China, and our campus pond (31°50'22.4" N, 117°15'23.4" E) were used as the natural waters. The tap water samples were obtained from the drinking water supply system of our campus. These samples were filtered twice through 0.20 μm hydrophilic PTFE filters (produced by Tianjin Fuji Technology Co., China) to remove suspended solids. A standard additive recovery method was used to measure the NB in these real water samples.

3. Results and discussion

3.1. Terminating the photoreduction of NB catalyzed by EY

As shown in Fig. 1a-d, solutions containing EY and NB had a central band at 517 nm, with a shoulder at 490 nm in the initial spectra attributable to the dimer EY [27]. Upon irradiation in the presence of dissolved oxygen, EY could be effectively decolorized in NB solutions, exhibiting pseudo-first-order kinetics. Notably, the photoinduced decolorization of EY was conventionally ascribed to the debromination of EY [30]. However, the EY photobleaching observed in the EY/NB solution ($k_{app,\ EY\text{-}NB\text{-}O} = 456.78 \pm 16.82 \times 10^{-3}\ min^{-1}$) was

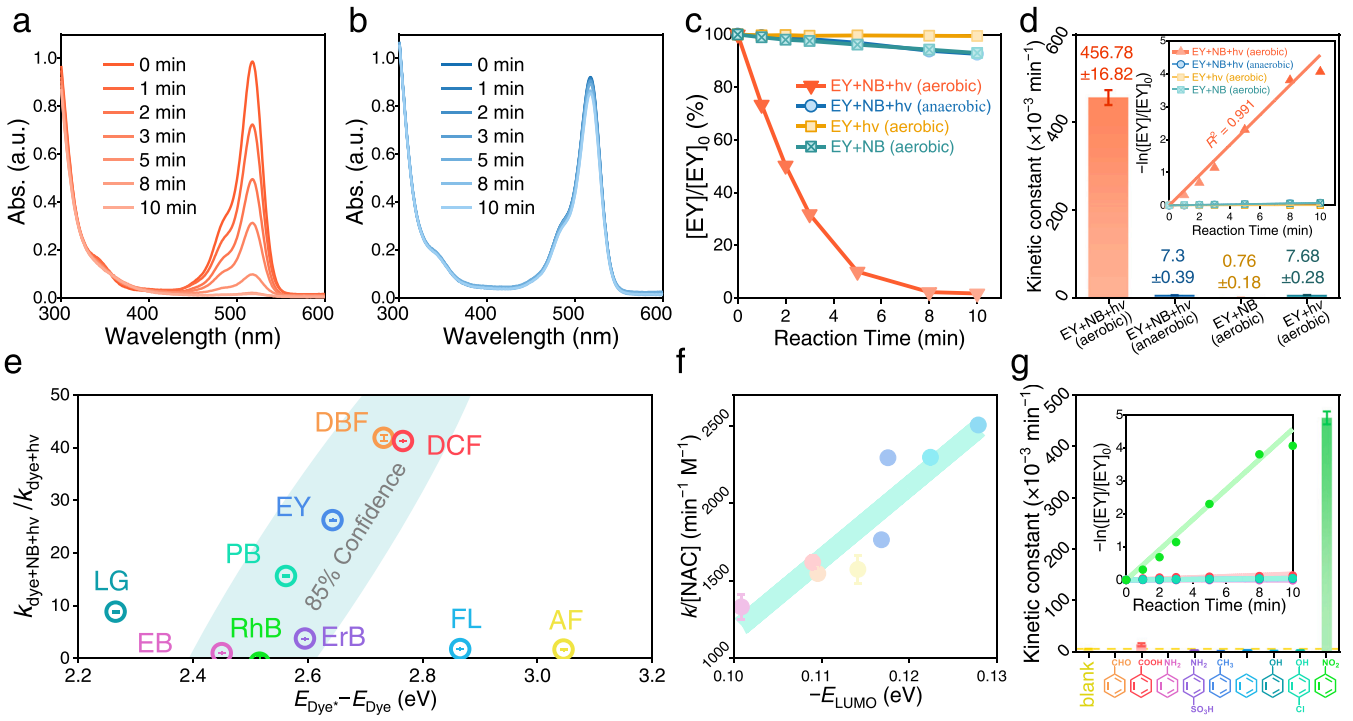

Fig. 1. (a-b) The variation curves of UV–Vis spectra of EY solution containing NB during irradiation under aerobic (a) and anaerobic conditions (b). (c) The photobleaching kinetics of EY and (d) the corresponding calculated apparent first-order kinetic constants (kapp). Conditions: [EY] = 10 μM, [NB] = 40 mg L^{-1}, irradiation intensity = 1.6 mW cm^{-2}. (e) Relationship between the excitation energies of different dyes and their responses to NB. Conditions: [dyes] = 10 μM, [NB] = 40 mg L^{-1}, irradiation intensity = 30 mW cm^{-2}. (f) Response of EY photobleaching to different NACs. (g) Comparison of EY photobleaching kinetics in the solutions of different aromatic compounds. Conditions: [EY] = 10 μM, [organics] = 40 mg L^{-1}, irradiation intensity = 1.6 mW cm^{-2}.

significantly faster than that in the EY solution ($k_{app,\ EY\text{-}O}$ = 7.30 ± 0.39 × 10^{-3} min^{-1}). After eliminating the dissolved oxygen from the EY/NB solution, the measured EY photobleaching rate decreased to a similar level to that in the EY solution ($k_{app,\ EY\text{-}NB}$ = 7.68 ± 0.28 × 10^{-3} min^{-1}). These results imply a new mechanism for EY photobleaching when the photocatalytic NB reduction was terminated in the presence of dissolved oxygen.

To reveal the possible structural selectivity of the dye fragmentation in the terminated photocatalytic NB reduction, the photodegradation of other dyes was monitored. In the presence of NB, all xanthene dyes were degraded after irradiation except eosin B (EB, X_1, X_2 = $–NO_2$, X_3, X_4 = –Br), while the other dyes showed no remarkable photobleaching under identical conditions (Figs. S2 and S3). For the quantification of NB, the k_{app} of NB-induced photobleaching should be 10 times higher than the k_{app} of self-photobleaching (i.e., noise in the kinetics) [31]. Bromination or chlorination would increase the photobleaching response of xanthene dyes to NB under irradiation, providing some alternative for detecting NB (Fig. S4). Such an increase in response might be due to the optimization of the excitation energy (i.e., $E_{dye^*} - E_{dye}$), and this could be tuned by changes in the substituent groups (Fig. 1e). These results suggest that the NB quenching of photoexcited dyes initiated NB-induced dye photobleaching. Reportedly, the efficiency and selectivity of $–NO_2$ reduction could be ensured in systems using EY as a photocatalyst [32], implying a selective reaction between the NB derivates and the excited dyes.

To verify that NAC could quench photoexcited EY (EY*) by accepting electrons, we further monitored the photodegradation of EY containing different NB derivatives. The presence of these NACs universally caused efficient EY decoloration, indicating that such a photodegradation could be attributed to the aromatic $–NO_2$ moieties. This result implies that this method might not distinguish the NACs in their mixed solutions. However, the photodegradation of EY showed different kinetics in different NAC solutions. As shown in Fig. 1f, the kinetic constants normalized by the NAC concentration were linearly correlated with the energies of their lowest unoccupied molecular orbitals (E_{LUMO}), indicating that the rate-determining step was the reduction of NAC by EY*. Such a finding also implied an important role of $–NO_2$ in the quenching process.

Despite the well-documented selectivity of EY-catalyzed NAC photoreduction [32], the effect of other aromatic organics without $–NO_2$ on this constructed photobleaching reaction remains unclear. To further show the selectivity of the EY photobleaching to the aromatic $–NO_2$ and demonstrate the feasibility of the developed detection method, the response of EY to different aromatic organics was also tested. As shown in Fig. 1g, the addition of different organic substrates into the EY solutions showed no significant difference in the measured photobleaching kinetic constants. Consequently, such an ultrafast photobleaching reaction could be used to indicate the presence of aromatic $–NO_2$ and was expected to be potentially used in complex aqueous substrates.

3.2. *Effects of photocatalytic parameters on the EY decoloration kinetics*

To assess the effect of experimental parameters on the sensitivity (i.e., the slope of the k_{app}-[NB] curve, $S_{k\text{-}[NB]}$) and LoD of NB quantification, the kinetics of EY decoloration under different photocatalytic conditions were investigated.

First, the role of irradiation intensity was analyzed. As the irradiation intensity increased from 0.3 to 3.2 mW cm^{-2}, $S_{k\text{-}[NB]}$ increased linearly from 9.60 ± 0.68–134.99 ± 4.07 × 10^{-3} L mg^{-1} min^{-1}, while the lowest LoD was obtained at an irradiation of 1.6 mW cm^{-2} (Fig. 2a). These findings indicate that the reaction between NB and EY* was the rate-determining step, and the change in irradiation intensity would alter the steady-state concentration of EY*. Thus, the increase in irradiation enhanced the response of EY to the changes in [NB], and it also raised the possibility of EY debromination, thus creating extra noise and reducing the accuracy of such a method.

The possible effect of EY concentration on the photobleaching kinetics was also explored. However, there was no visible change in the $S_{k\text{-}}$

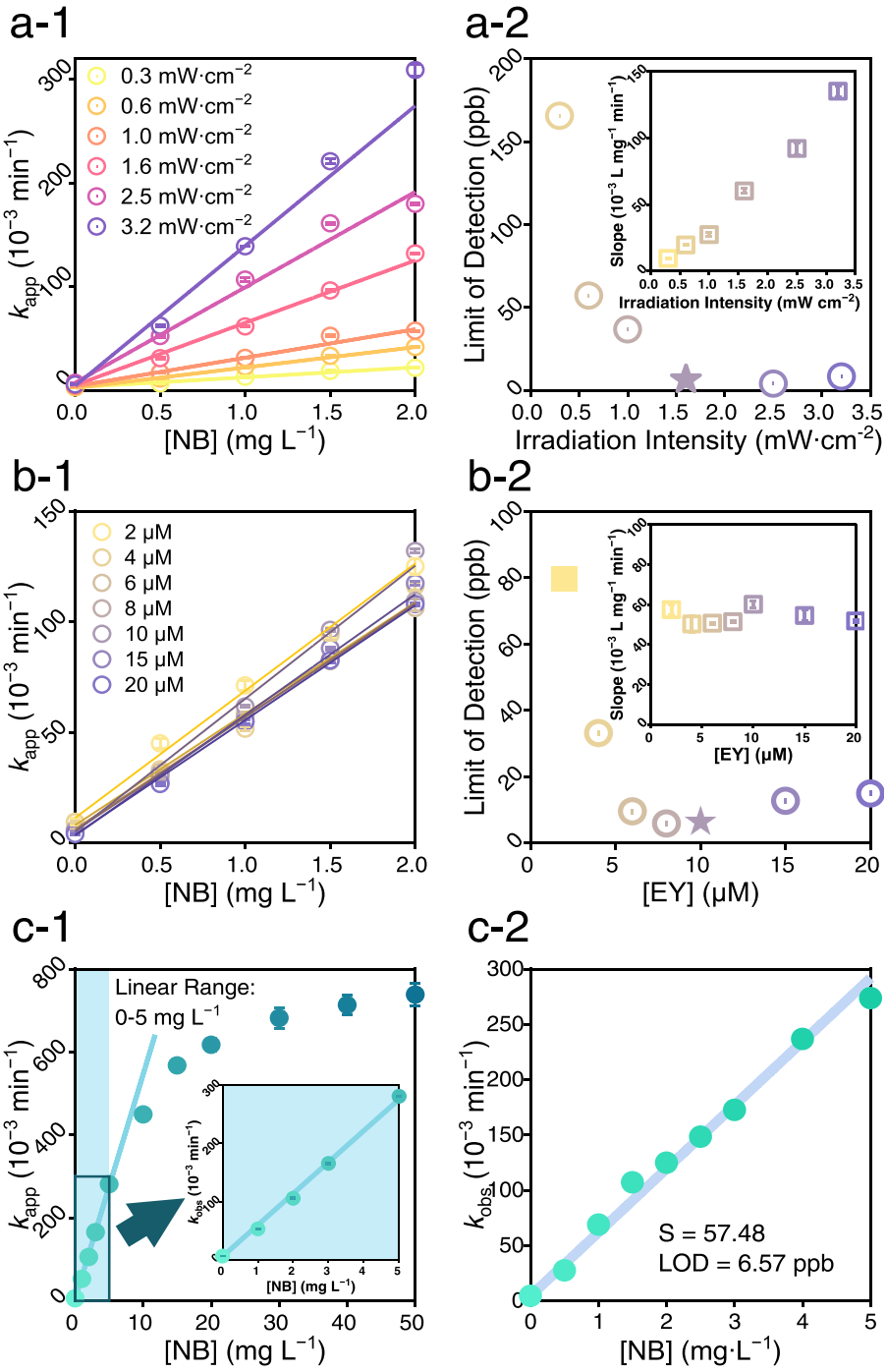

Fig. 2. Effects of (a) irradiation intensity and (b) EY concentration on the sensitivity and limit of detection (LoD) of the proposed detection method for NB. (c) Linear range and the corresponding LoD values measured under optimized conditions: [EY] = 10 μM, irradiation intensity = 1.6 mW cm^{-2}.

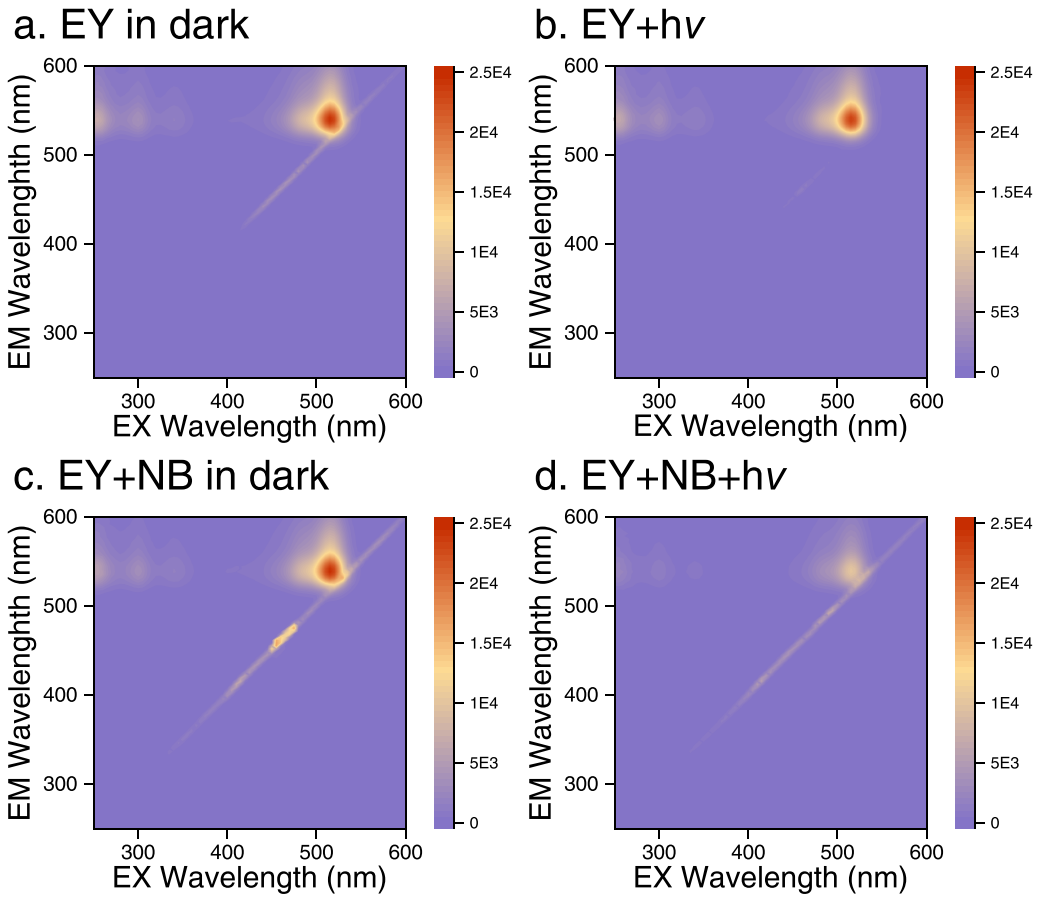

Fig. 3. The 3D fluorescence spectra of EY solutions (a) in the dark, (b) after light irradiation, and EY/NB solution (c) in the dark, (d) after light irradiation. Conditions: [EY] = 10 μM, [NB] = 40 mg L^{-1}, irradiation intensity = 1.6 mW cm^{-2}. Colorbar indicates the intensity of fluorescence.

$_{[NB]}$ value when the EY concentration increased from 2 to 20 μM (Figs. 2b and S5), implying the minor role of EY concentration. Considering that EY was continuously fragmented during NB detection, a high concentration of EY might be beneficial to maintain a constant steady-state concentration of EY*. Additionally, the high concentration of EY might interfere with the in-situ measurement of absorbance. Overall, the lowest LoD was obtained at an EY concentration of 10 μM.

Moreover, the target contaminant NB might also affect the reliability of the detection, and thus, its influence also needs to be revealed. As the NB concentration was increased from 0 to 50 mg L^{-1}, a high concentration of NB was observed to disrupt the steady state of EY* generation, thus showing a nonlinear relationship with k_{app} (Fig. 2c-1). However, at a low NB concentration ($\leq$ 5 mg L^{-1}), the feasibility of this quantitation detection based on the linear relationship between k_{app} and [NB] for EY photobleaching could be ensured. As shown in Fig. 2c-2, this proposed method was confirmed to provide a sensitive and reliable quantitative assessment of NB concentrations (LoD = 6.57 ppb, R^2 = 0.991). The LoD was lower than that of the recently reported spectral methods for NAC quantification [8,14,33,34] and was similar to that of the most sensitive electrochemical methods [9,35]. Additionally, it was also capable of accurately detecting contaminants of widespread concern with aromatic –NO_2, such as picric acid, chloramphenicol, and metronidazole (Fig. S6).

When applying this method to detect NACs in environmental samples, the different concentrations of dissolved oxygen might affect the response of EY photobleaching to [NB] change. To accurately quantify NACs in these actual samples, these samples were shaked for 1 min to make the amount of O_2 reach the equilibrium concentration. As shown in Fig. S7, the response of EY photobleaching to [NB] change was ensured at a similar level after shaking. Such a simple procedure could effectively ensure the accuracy and feasibility of this quantitation method.

3.3. Fragmentation pathway of EY

The complete decay of visible-light absorption initially indicated the fragmentation of the eosin chromophore. Moreover, the fluorescence excitation-emission matrix (EEM) spectra of the unirradiated EY solutions (Fig. 3a) show a characteristic peak of EY at ~515 nm (excitation)/ ~538 nm (emission) [36]. After irradiation or dosing NB (Fig. 3b and c), no obvious shift or decrease in intensity was observed in the maximum emission. However, in the EY/NB system, the peak disappeared rapidly upon irradiation (Fig. 3d). These findings suggest that unlike the well-documented eosin photobleaching caused by photoinduced dehalogenation, the eosin chromophore was highly fragmented in the constructed semi-cycle photocatalysis [37].

To further explore the fragmentation pathways of EY in the constructed EY/NB system, LC–MS was used to identify the possible products (Fig. 4). Similar to the above results, photoinduced debromination products were not detected [27]. Instead, the EY was fragmented into two products via a two-step pathway, including (i) the hydration of the most active C═C located in the LUMO of the EY and (ii) the fragmentation of the hydrated EY (Scheme 1a). Notably, these products show no visible-light absorbance in the simulated UV–Vis spectra (Fig. 5a). Thus, this selective breaking of the eosin chromophore induced a rapid discoloration of EY and allowed a reliable kinetic analysis.

3.4. Mechanism of the semi-cycle photocatalysis

Remarkably, the EY-based photocatalytic mechanism has been intensively studied, providing massive descriptions of the EY behavior in

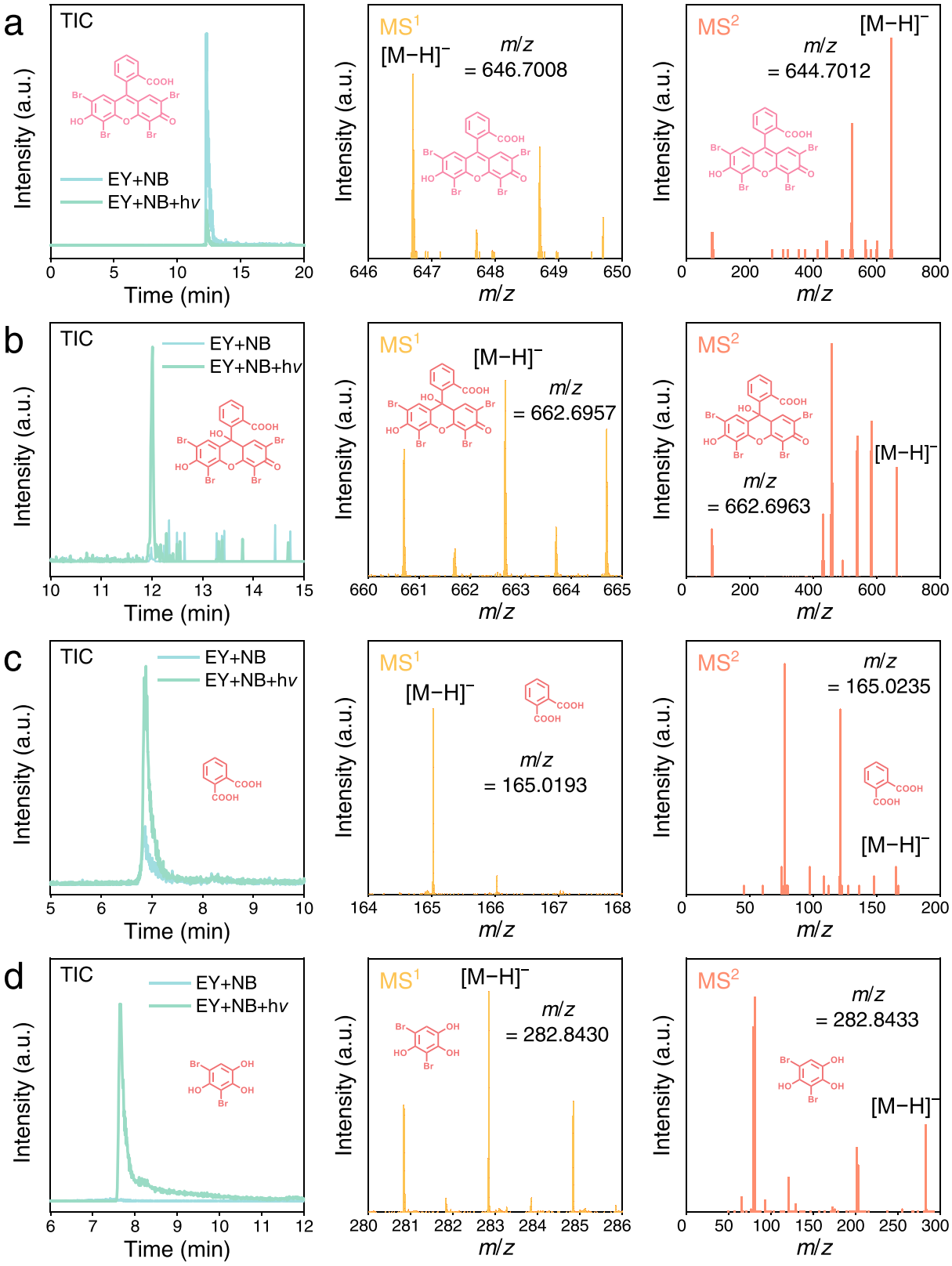

Fig. 4. Identification of EY photobleached products using LC–MS/MS analysis. (a) EY; (b-d) photobleaching products.

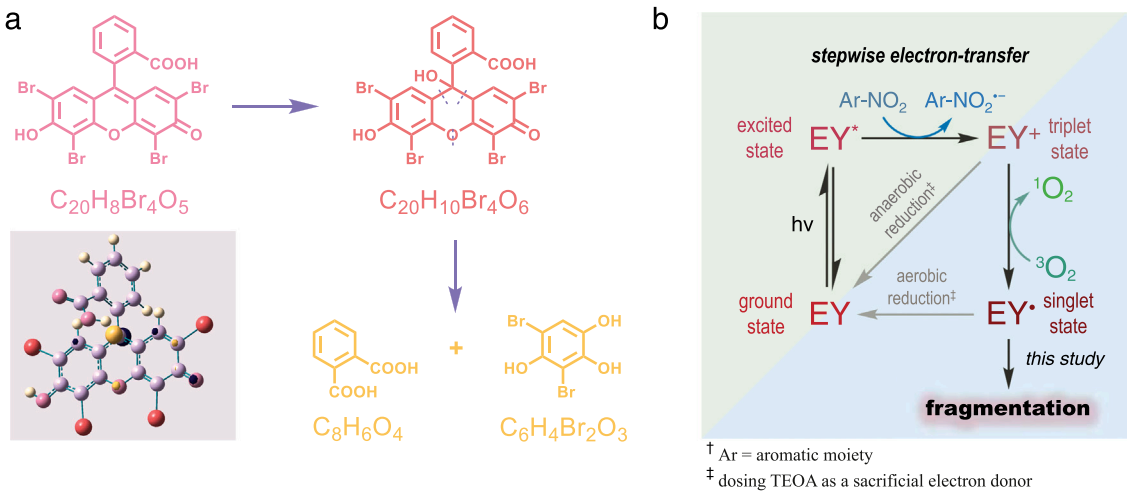

Scheme 1. (a) The fragmentation pathway of EY after irradiation in a solution containing NB. (b) A proposed mechanism of ultrafast EY photobleaching in the presence of nitrobenzene and dissolved oxygen.

light-driven processes [38,39]. With these results, the photobleaching mechanism of EY in such a semi-cycle relying on the presence of NACs was elucidated.

As shown in Fig. 1b, the fragmentation of EY was completely suppressed when dissolved oxygen was removed from the EY/NB solution, indicating the crucial role of O_2 in NB-induced EY photobleaching. Moreover, 2,2,6,6-tetramethylpiperidine (TEMP) was converted into a product that captured the $^1O_2$ (i.e., TEMPO) upon irradiation of the aerobic EY/NB system during the in situ EPR analysis, suggesting the continuous generation of $^1O_2$ (Fig. 5b). This reaction between photoexcited EY and dissolved dioxygen was reported to produce highly active $^1O_2$ and EY$^\bullet$ [40,41]. In the EY/NB system, the generation rates of both products were enhanced by the effective quenching of EY* by NB. Next, EY$^\bullet$ further reacted with the surrounding solvent and was then rapidly fragmented.

To examine the hypothesis that NB was involved in the quenching of EY*, the emission lifetimes of EY* in the presence of different organics were measured. As shown in Fig. 5c-1, the lifetime of EY* shortened from 1.042 ns to 1.008 ns in the presence of NB, while other organics failed to shorten its lifetime. This result suggests that NB could efficiently accept electrons from EY* [42]. Moreover, when a commonly sacrificial electron donor of triethanolamine (TEOA) was dosed, the EY* lifetime was recovered to 1.041 ns (Fig. 5c-2). Thus, the decrease in the EY* lifetime was due to a selective redox reaction between EY* and NB.

To further prove that NB enabled EY^+ generation by quenching EY*, the transient photocurrent responses of the EY solution in the presence or absence of NB were monitored. As shown in Fig. 5d, the photocurrent increased significantly from 0.03 μA to 4.45 μA after the addition of NB to the EY solution. Thus, the transition from EY to the positively charged EY^+ was initially forbidden but was enabled by dosing NB. This result well supports the formation of EY^+ followed by EY* quenching.

Taken together, we proposed a plausible mechanism for EY photobleaching in the presence of NB (Scheme 1b) as follows: (i) first, the excited state EY (EY*) is generated under visible-light irradiation; (ii) then, EY* could selectively reduce NB, which would be converted to positively charged EY^+ (triplet) via a stepwise electron transfer mechanism [32]; and (iii) finally, the dissolved oxygen efficiently quenches EY^+ and further generates highly reactive EY$^\bullet$. Both the generated EY^+ and EY$^\bullet$ could be reduced to the ground-state EY, ensuring the general stability of EY in conventional photocatalysis [23,32]. However, when the supply of extra sacrificial electron donors was cut off, the EY^+ could reversibly return to their ground state. At the same time, the reactive EY$^\bullet$ rapidly split into colorless products. As a result, such a selective response might provide a new method for quantitatively detecting NB and other NACs in aqueous solutions.

3.5. Application of the methods to quantify NACs in water samples

Complex solutes in water may interfere with the quantitation of NACs and compromise the sensitivity and selectivity of this detection method. Indispensably, the anti-interference and practical performance of this method were also tested.

Notably, the pH will determine the equilibrium of protic and isomeric solutes in aqueous EY solutions, thus affecting the UV–Vis spectra of EY solutions.[43,44] Thus, a low pH markedly increased the $S_{k\text{-[NB]}}$ of this method to further improve the sensitivity of this method (Fig. 5a). However, the strong acid condition (pH $\leq$ 3.0) might reduce the solubility of EY and accelerate its aggregation [45,46]. Therefore, when applying this method to detect NACs in actual water samples, we used a phthalate buffer (50 mM) to maintain the pH at 4.0.

The practicality of this NAC detection method was verified by testing in systems containing different ions or water sources. As shown in Fig. 6b and c, the interference of these additive cations and anions on the $S_{k\text{-[NB]}}$ values for NB quantitation was negligible. Moreover, the presence of transition metals also had a minor influence, except for Cu^{2+} (Fig. 6d). This ineffectiveness caused by Cu^{2+} could be attributed to the formation of a Cu(II)-EY complex via –COOH, enabling a rapid intramolecular electron/energy transfer and thus self-quenching of its fluorescence [47,48]. To ensure the practical feasibility of this method, ethylenediaminetetraacetate (EDTA) was used as the masking agent for Cu^{2+} [49]. As shown in Fig. 7, although Cu^{2+} remarkably inhibited the EY photobleaching in NB solution, the strong masking effect of EDTA completely recover the response of EY photobleaching to [NB].

Regarding the effect of different water sources, deionized water, tap water, water from our campus lakes, and Chaohu Lake were chosen as water distribution studies. Interestingly, the recoveries for these actual samples ranged from 91.57% to 107.62%, with relative standard deviations (RSDs) ranging from 2.96% to 5.78% (Table 3). These results reconfirm the feasibility and reliability of this method for practical applications.

4. Conclusions

In this work, we proposed a new approach to choosing a widely studied photosensitizer as a highly efficient and selective probe for NAC detection. The EY* quenching by NACs was observed to further cause ultrafast EY decoloration in the constructed semi-cycle photocatalysis by terminating the supply of sacrificial electron donors. The mechanism for

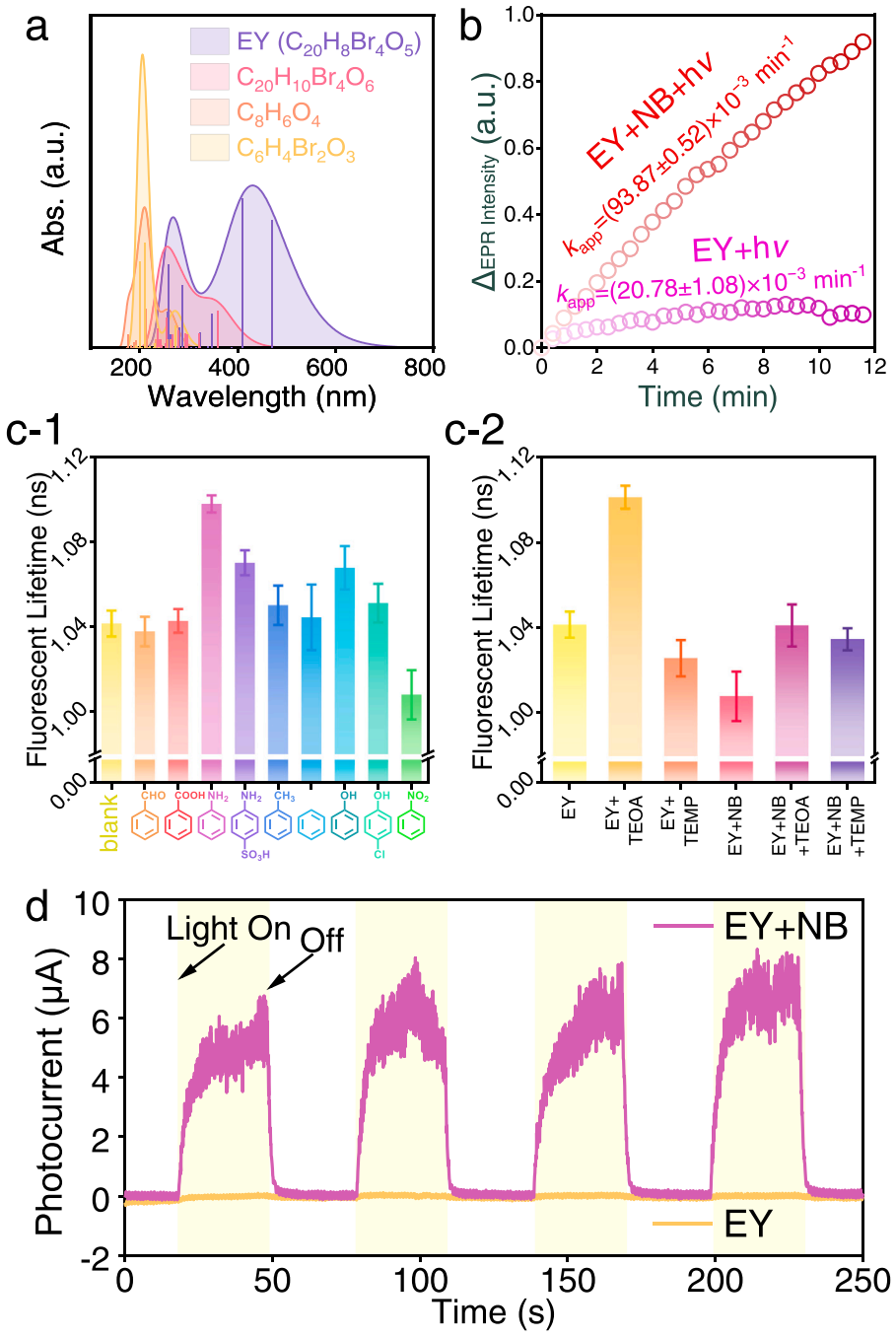

Fig. 5. (a) UV–vis spectra of EY and photobleaching products simulated using a Gaussian function with a half-width of 3000 cm^{-1}. (b) The variation curves of TEMPO intensities in EY and EY/NB solutions. (c) Analysis of the fluorescence lifetime of EY in different solutions. Conditions: [EY] = 1 μM, [NB] = 20 mg L^{-1}, [organics] = [TEOA] = [TEMP] = 10 μM. (d) Transient photocurrent responses of EY and EY/NB solutions. Conditions: [EY] = 50 μM, [NB] = 20 mg L^{-1}.

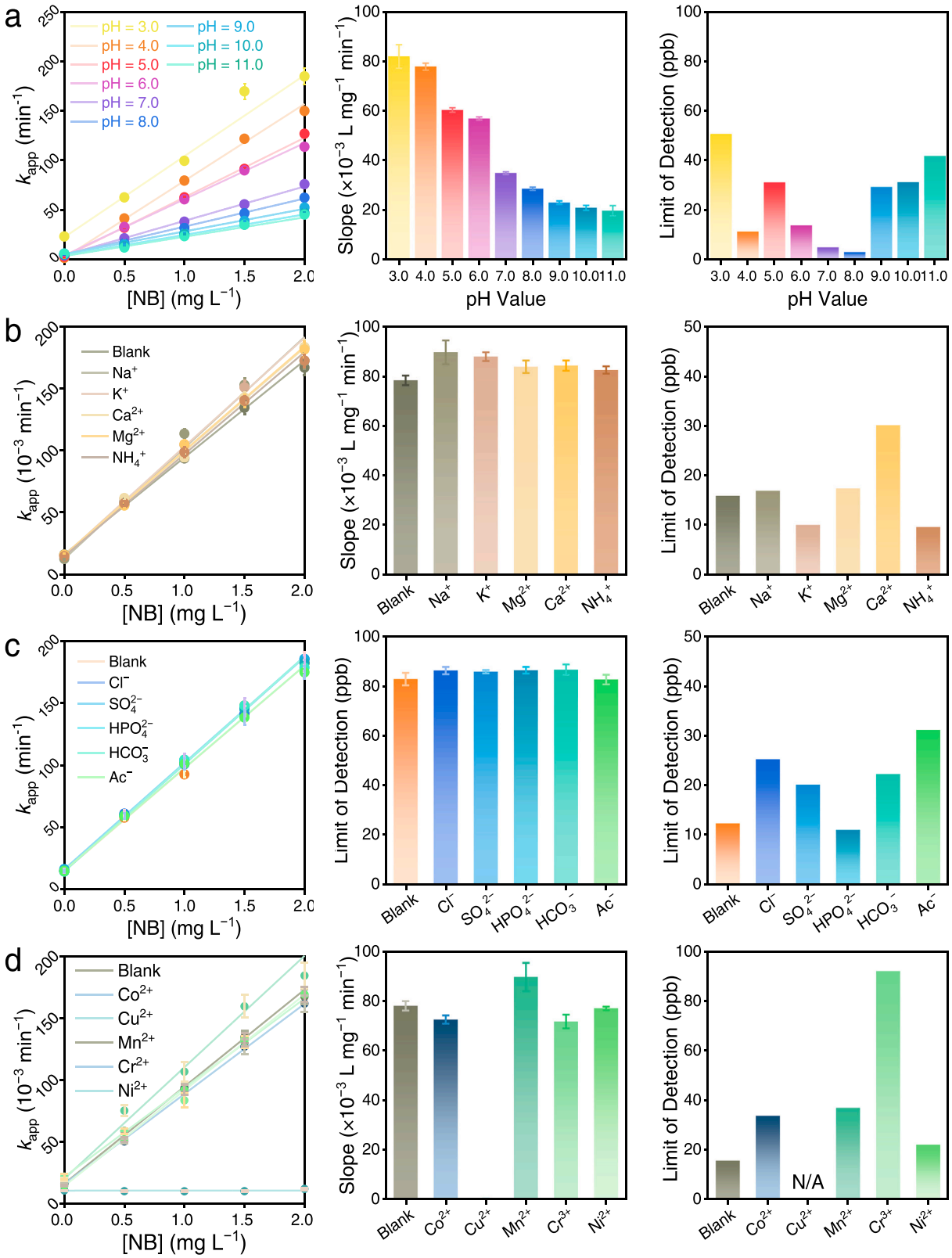

Fig. 6. (a) Effect of pH on NB detection. Conditions: [EY] = 10 μM, irradiation intensity = 1.6 mW cm^{-2}. Effects of different (b) cations (hydrochloride), (c) anions (potassium salt), and (d) transition metal ions (hydrochloride) on NB detection. Conditions: [EY] = 10 μM, irradiation intensity = 1.6 mW cm^{-2}, [pH] = 4.0.

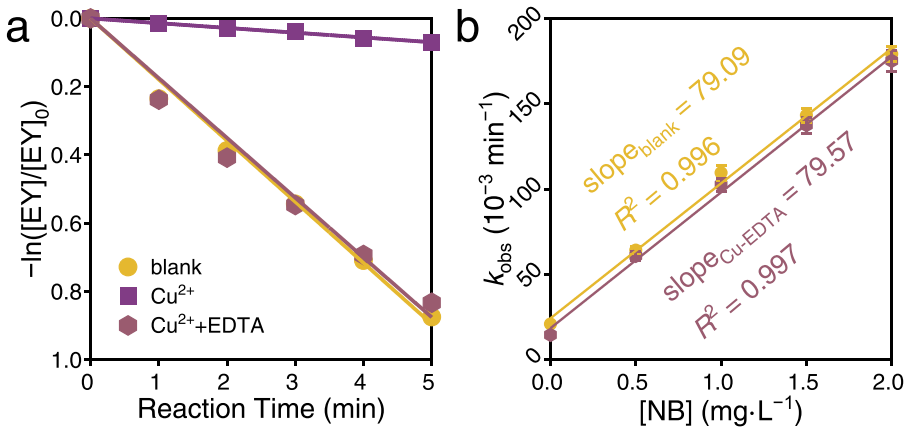

Fig. 7. (a) The photobleaching kinetics of EY in the presence of Cu^{2+} and EDTA. Conditions: [NB] = 2 mg L^{-1}. (b) NB detection in the presence of EDTA as a masking agent for Cu^{2+}. Conditions: [EY] = 10 μM, [Cu^{2+}] = 10 μM, [EDTA] = 100 μM, irradiation intensity = 1.6 mW cm^{-2}, [pH] = 4.0.

Table 3
Detection of NB in various water sources.

Sample	NB concentration (mg L^{-1}) dosed	measured	Recovery (%)	RSD (%)
tap water	0.5	0.53 ± 0.02	106.51	4.67
	1	0.99 ± 0.04	99.23	4.23
	1.5	1.51 ± 0.06	100.74	3.79
	2	1.94 ± 0.07	96.95	3.40
campus pond	0.5	0.54 ± 0.03	107.62	5.78
	1	1.00 ± 0.04	100.14	3.77
	1.5	1.51 ± 0.05	100.34	3.71
	2	1.91 ± 0.07	95.55	3.68
Chao Lake 1	0.5	0.52 ± 0.02	103.37	4.41
	1	1.02 ± 0.03	101.79	3.58
	1.5	1.37 ± 0.04	91.57	3.12
	2	1.87 ± 0.04	93.52	2.19
Chao Lake 2	0.5	0.50 ± 0.02	100.40	4.23
	1	0.98 ± 0.04	97.68	4.01
	1.5	1.54 ± 0.05	102.99	3.75
	2	1.90 ± 0.06	94.82	2.96

such a rapid photoinduced EY fragmentation could be attributed to the generation of highly reactive $EY^{\bullet}$. By monitoring the kinetics of EY decoloration, a facile but sensitive and accurate method was then developed for selective NAC detection, showing lower LoD values compared to the other reported electrochemical methods. Moreover, such a method exhibited a robust resistance to the interface when detecting NACs in complex water matrices. By reducing the complex process of synthesizing probes or electrode materials, this unique commercially available dye will provide an easy-to-use and standardizable method for NAC detection.

CRediT authorship contribution statement

Jing-Hang Wu, Tian-Hao Yang and Han-Qing Yu conceived and planned the experiments. Jing-Hang Wu and Tian-Hao Yang carried out the relative experiments. Jing-Hang Wu, Tian-Hao Yang and Fei Chen conducted and analyzed the various characterizations. Jing-Hang Wu wrote the initial draft of the manuscript, and further modified by Feng Zhang, Jie-Jie Chen and Han-Qing Yu. All authors have given approval to the final version of the manuscript.

Declaration of Competing Interest

The authors declare that they have no known competing financial interests or personal relationships that could have appeared to influence the work reported in this paper.

Data availability

Data will be made available on request.

Acknowledgments

The authors thank the National Natural Science Foundation of China (51821006, 52027815 and 52192684). Additionally, the authors acknowledge Dr. Yuan Min and Dr. Bo Gong for their help in performing the quantum chemical calculations.

Appendix A. Supplementary material

Supplementary data associated with this article can be found in the online version at doi:10.1016/j.apcatb.2023.122363.

References

[1] G. Booth, Nitro compounds, aromatic. Ullmann's Encyclopedia of Industrial Chemistry, Wiley-VCH, Weinheim, 2005.
[2] F. Zapata, C. García-Ruiz, Chemical classification of explosives, Crit. Rev. Anal. Chem. 51 (2021) 656–673, https://doi.org/10.1080/10408347.2020.1760783.
[3] X. Li, R.R. Thakore, B.S. Takale, F. Gallou, B.H. Lipshutz, High turnover Pd/C Catalyst for nitro group reductions in water. One-pot sequences and syntheses of pharmaceutical intermediates, Org. Lett. 23 (2021) 8114–8118, https://doi.org/10.1021/acs.orglett.1c03258.
[4] J. Sun, H. Wang, C. Zheng, G. Wang, Synthesis of some surfactant-type acid dyes and their low-temperature dyeing properties on wool fiber, J. Clean. Prod. 218 (2019) 284–293, https://doi.org/10.1016/j.jclepro.2019.01.341.
[5] N. Wang, G. Lv, L. He, X. Sun, New insight into photodegradation mechanisms, kinetics and health effects of *p*-nitrophenol by ozonation in polluted water, J. Hazard. Mater. 403 (2021), 123805, https://doi.org/10.1016/j.jhazmat.2020.123805.
[6] M. Bilal, A.R. Bagheri, P. Bhatt, S. Chen, Environmental occurrence, toxicity concerns, and remediation of recalcitrant nitroaromatic compounds, J. Environ. Manag. 291 (2021), 112685, https://doi.org/10.1016/j.jenvman.2021.112685.
[7] E. Hussain, Y. Li, C. Cheng, H. Zhuo, S.A. Shahzad, S. Ali, M. Ismail, H. Qi, C. Yu, Benzo[ghi]perylene and coronene as ratiometric fluorescence probes for the selective sensing of nitroaromatic explosives, Talanta 207 (2020), 120316, https://doi.org/10.1016/j.talanta.2019.120316.
[8] H. Zheng, Y.K. Deng, M.Y. Ye, Q.F. Xu, X.J. Kong, L.S. Long, L.S. Zheng, Lanthanide-titanium oxo clusters as the luminescence sensor for nitrobenzene detection, lnorg. Chem. 59 (2020) 12404–12409, https://doi.org/10.1021/acs.inorgchem.0c01494.
[9] C. Liu, X. Bo, L. Guo, A novel electrochemical sensing platform of JUC-62 metal-organic framework/platelet ordered mesoporous carbon for high selective detection of nitro-aromatic compounds, Sens. Actuators B Chem. 297 (2019), 126741, https://doi.org/10.1016/j.snb.2019.126741.
[10] P. Kumar, K.H. Kim, P.K. Mehta, L. Ge, G. Lisak, Progress and challenges in electrochemical sensing of volatile organic compounds using metal-organic frameworks, Crit. Rev. Environ. Sci. Technol. 49 (2019) 2016–2048, https://doi.org/10.1080/10643389.2019.1601489.
[11] H. Chu, L. Yang, L. Yu, J. Kim, J. Zhou, M. Li, J.S. Kim, Fluorescent probes in public health and public safety, Coord. Chem. Rev. 449 (2021), https://doi.org/10.1016/j.ccr.2021.214208.

[12] S.A. Gungor, I. Sahin, O. Gungor, S.E. Kariper, F. Tumer, M. Kose, Pamoic acid esters and their xanthene derivatives: flourimetric detection of nitroaromatic compounds and non-linear optical properties, Sens. Actuators B Chem. 255 (2018) 3344–3354, https://doi.org/10.1016/j.snb.2017.09.161.
[13] M. Fan, B. Sun, X. Li, Q. Pan, J. Sun, P. Ma, Z. Su, Highly fluorescent cadmium based metal–organic frameworks for rapid detection of antibiotic residues Fe^{3+} $Cr_2O_7^{2-}$ ions, lnorg. Chem. 60 (2021) 9148–9156, https://doi.org/10.1021/acs.inorgchem.1c01165.
[14] S.H. Chen, S.H. Luo, L.J. Xing, K. Jiang, Y.P. Huo, Q. Chen, Z.Y. Wang, Rational design and facile synthesis of dual-state emission fluorophores: expanding functionality for the sensitive detection of nitroaromatic compounds, Chem. Eur. J. 28 (2022), e202103478, https://doi.org/10.1002/chem.202103478.
[15] F. Afshariazar, A. Morsali, A dual-response regenerable luminescent 2D-MOF for nitroaromatic sensing via target-modulation of active interaction sites, J. Mater. Chem. C 9 (2021) 12849–12858, https://doi.org/10.1039/D1TC02190G.
[16] E. Rampler, Y.E. Abiead, H. Schoeny, M. Rusz, F. Hildebrand, V. Fitz, G. Koellensperger, Recurrent topics in mass spectrometry-based metabolomics and lpidomics: standardization, coverage, and throughput, Anal. Chem. 93 (2021) 519–545, https://doi.org/10.1021/acs.analchem.0c04698.
[17] Z.N. Hu, J. Liang, K. Ding, Y. Ai, Q. Liang, H.B. Sun, Insight into the selectivity of nano-catalytic nitroarenes reduction over other active groups by exploring hydrogen sources and metal components, Appl. Catal. A Gen. 626 (2021), 118339, https://doi.org/10.1016/j.apcata.2021.118339.
[18] D. Formenti, F. Ferretti, F.K. Scharnagl, M. Beller, Reduction of nitro compounds using 3d-non-noble metal catalysts, Chem. Rev. 119 (2019) 2611–2680, https://doi.org/10.1021/acs.chemrev.8b00547.
[19] J. Song, Z.F. Huang, L. Pan, K. Li, X. Zhang, L. Wang, J.J. Zou, Review on selective hydrogenation of nitroarene by catalytic, photocatalytic and electrocatalytic reactions, Appl. Catal. B Environ. 227 (2018) 386–408, https://doi.org/10.1016/j.apcatb.2018.01.052.
[20] A. Cheruvathoor Poulose, G. Zoppellaro, I. Konidakis, E. Serpetzoglou, E. Stratakis, O. Tomanec, M. Beller, A. Bakandritsos, R. Zbořil, Fast and selective reduction of nitroarenes under visible light with an earth-abundant plasmonic photocatalyst, Nat. Nanotechnol. 17 (2022) 485–492, https://doi.org/10.1038/s41565-022-01087-3.
[21] J. Wang, R. Huang, W. Qi, R. Su, B.P. Binks, Z. He, Construction of a bioinspired laccase-mimicking nanozyme for the degradation and detection of phenolic pollutants, Appl. Catal. B Environ. 254 (2019) 452–462, https://doi.org/10.1016/j.apcatb.2019.05.012.
[22] V.J. Roy, P.P. Sen, S.R. Roy, Exploring eosin Y as a bimodular catalyst: organophotoacid mediated Minisci-type acylation of *N*-heteroarenes, Chem. Commun. 58 (2022) 1776–1779, https://doi.org/10.1039/D1CC06483E.
[23] J.H. Wu, F. Zhang, Rapid aerobic visible-light-driven photo-reduction of nitrobenzene, Sci. Total Environ. 710 (2020), 136322, https://doi.org/10.1016/j.scitotenv.2019.136322.
[24] T. Hering, A.U. Meyer, B. König, Photocatalytic anion oxidation and applications in organic synthesis, J. Org. Chem. 81 (2016) 6927–6936, https://doi.org/10.1021/acs.joc.6b01050.
[25] N.E.S. Tay, D. Lehnherr, T. Rovis, Photons or electrons? A critical comparison of electrochemistry and photoredox catalysis for organic synthesis, Chem. Rev. 122 (2022) 2487–2649, https://doi.org/10.1021/acs.chemrev.1c00384.
[26] J. Wang, Y. Liu, Y. Li, L. Xia, M. Jiang, P. Wu, Highly efficient visible-light-driven H_2 production via an eosin Y-based metal–organic framework, lnorg. Chem. 57 (2018) 7495–7498, https://doi.org/10.1021/acs.inorgchem.8b00718.
[27] A. Alvarez-Martin, S. Trashin, M. Cuykx, A. Covaci, K. De Wael, K. Janssens, Photodegradation mechanisms and kinetics of eosin-Y in oxic and anoxic conditions, Dyes Pigment. 145 (2017) 376–384, https://doi.org/10.1016/j.dyepig.2017.06.031.
[28] M. Enoki, R. Katoh, Estimation of quantum yields of weak fluorescence from eosin Y dimers formed in aqueous solutions, Photochem. Photobiol. Sci. 17 (2018) 793–799, https://doi.org/10.1039/c7pp00465f.
[29] F. Chen, L.L. Liu, Y.J. Zhang, J.H. Wu, G.X. Huang, Q. Yang, J.J. Chen, H.Q. Yu, Enhanced full solar spectrum photocatalysis by nitrogen-doped graphene quantum dots decorated BiO_{2-x} nanosheets: ultrafast charge transfer and molecular oxygen activation, Appl. Catal. B Environ. 277 (2020), 119218, https://doi.org/10.1016/j.apcatb.2020.119218.
[30] I. Groeneveld, S.E. Schoemaker, G.W. Somsen, F. Ariese, M.R. van Bommel, Characterization of a liquid-core waveguide cell for studying the chemistry of light-induced degradation, Analyst 146 (2021) 3197–3207, https://doi.org/10.1039/D1AN00272D.
[31] A.A. Alinaghi Langari, S. Alizadeh, S. Soury, A. Firoozichahak, D. Nematollahi, P. M. Alizadeh, N. Sanaei, Nano-hydroxyapatite/polyaniline composite as an efficient sorbent for sensitive determination of the polycyclic aromatic hydrocarbons in air by a needle trap device, RSC Adv. 10 (2020) 42267–42276, https://doi.org/10.1039/D0RA07540J.
[32] X.J. Yang, B. Chen, L.Q. Zheng, L.Z. Wu, C.H. Tung, Highly efficient and selective photocatalytic hydrogenation of functionalized nitrobenzenes, Green Chem. 16 (2014) 1082–1086, https://doi.org/10.1039/C3GC42042F.
[33] M. Cao, C. Xia, Y. Liu, J. Xia, D. Jiang, G. Zhou, T. Xuan, H. Li, Bifunctional color-tuning luminescent Ln@Zr-MOFs for white LEDs and sensitive, ultrafast detection of nitrobenzene in aqueous media, J. Mater. Chem. C 10 (2022) 1690–1697, https://doi.org/10.1039/D1TC05243H.
[34] X. Quan, X. Xu, B. Yan, Facile fabrication of Tb^{3+}-functionalized COF mixed-matrix membrane as a highly sensitive platform for the sequential detection of oxolinic acid and nitrobenzene, J. Hazard. Mater. 427 (2022), 127869, https://doi.org/10.1016/j.jhazmat.2021.127869.
[35] M.M. Ruiz-Ramirez, C. Silva-Carrillo, J.J. Hinostroza-Mojarro, Y.Y. Rivera-Lugo, P. Valle-Trujillo, B. Trujillo-Navarrete, Electrochemical sensor for determination of nitrobenzene in aqueous solution based on nanostructures of TiO_2/GO, Fuel 283 (2021), 119326, https://doi.org/10.1016/j.fuel.2020.119326.
[36] T. Wen, N.B. Li, H.Q. Luo, A turn-on fluorescent sensor for sensitive and selective detection of sodium dodecyl sulfate based on the eosin Y/polyethyleneimine system, Anal. Chem. 85 (2013) 10863–10868, https://doi.org/10.1021/ac402241m.
[37] P.G. Lynch, H. Richards, K.L. Wustholz, Unraveling the excited-state dynamics of eosin Y photosensitizers using single-molecule spectroscopy, J. Phys. Chem. A 123 (2019) 2592–2600, https://doi.org/10.1021/acs.jpca.9b00409.
[38] D.P. Hari, B. König, Synthetic applications of eosin Y in photoredox catalysis, Chem. Commun. 50 (2014) 6688–6699, https://doi.org/10.1039/C4CC00751D.
[39] D.M. Yan, J.R. Chen, W.J. Xiao, New roles for photoexcited eosin Y in photochemical reactions, Angew. Chem. Int. Ed. 58 (2019) 378–380, https://doi.org/10.1002/anie.201811102.
[40] F. Xue, W. Du, S. Chen, M. Ma, Y. Kuang, J. Chen, T. Yi, H. Chen, Hypoxia-induced photogenic radicals by eosin Y for efficient phototherapy of hypoxic tumors, ACS Appl. Bio Mater. 3 (2020) 8962–8969, https://doi.org/10.1021/acsabm.0c01223.
[41] L.V. Lutkus, S.S. Rickenbach, T.M. McCormick, Singlet oxygen quantum yields determined by oxygen consumption, J. Photochem. Photobiol. A Chem. 378 (2019) 131–135, https://doi.org/10.1016/j.jphotochem.2019.04.029.
[42] A. Lewandowska-Andrałojć, D. Larowska, E. Gacka, T. Pedzinski, B. Marciniak, How eosin Y/graphene oxide-based materials can improve efficiency of light-driven hydrogen generation: mechanistic aspects, J. Phys. Chem. C 124 (2020) 2747–2755, https://doi.org/10.1021/acs.jpcc.9b09573.
[43] C.F. de Freitas, B.M. Estevão, D.S. Pellosi, I.S. Scarminio, W. Caetano, N. Hioka, V. R. Batistela, Chemical equilibria of eosin Y and its synthetic ester derivatives in non-ionic and ionic micellar environments, J. Mol. Liq. 327 (2021), 114794, https://doi.org/10.1016/j.molliq.2020.114794.
[44] D. Vanzin, C.F. Freitas, D.S. Pellosi, V.R. Batistela, A.E.H. Machado, R.M. Pontes, W. Caetano, N. Hioka, Experimental and computational studies of protolytic and tautomeric equilibria of erythrosin B and eosin Y in water/DMSO, RSC Adv. 6 (2016) 110312–110328, https://doi.org/10.1039/C6RA12198E.
[45] S. Kim, A. Martínez Dibildox, A. Aguirre-Soto, H.D. Sikes, Exponential amplification using photoredox autocatalysis, J. Am. Chem. Soc. 143 (2021) 11544–11553, https://doi.org/10.1021/jacs.1c04236.
[46] S. De, S. Das, A. Girigoswami, Environmental effects on the aggregation of some xanthene dyes used in lasers, Spectrochim. Acta A Mol. Biomol. Spectrosc. 61 (2005) 1821–1833, https://doi.org/10.1016/j.saa.2004.06.054.
[47] R. Kaushik, R. Sakla, A. Ghosh, S. Dama, A. Mittal, D.A. Jose, Copper complex-embedded vesicular receptor for selective detection of cyanide ion and colorimetric monitoring of enzymatic reaction, ACS Appl. Mater. Interfaces 11 (2019) 47587–47595, https://doi.org/10.1021/acsami.9b17316.
[48] H. Shi, Y. Cui, Y. Gong, S. Feng, Highly sensitive and selective fluorescent assay for guanine based on the Cu^{2+}/eosin Y system, Spectrochim. Acta A Mol. Biomol. Spectrosc. 161 (2016) 150–154, https://doi.org/10.1016/j.saa.2016.02.023.
[49] G.D. Christian, P.K. Dasgupta, K.A. Schug, Complexometric reactions and titrations. Analytical Chemistry, John Wiley & Sons, 2013, pp. 322–341.